

# Precise Time and Conditions of Peak Taconian Granulite Facies Metamorphism in the Southern Appalachian Orogen, U.S.A., with Implications for Zircon Behavior during Crustal Melting Events

David P. Moecher, Scott D. Samson,<sup>1</sup> and Calvin F. Miller<sup>2</sup>

University of Kentucky, Department of Geological Sciences, Lexington, Kentucky 40506, U.S.A.  
(e-mail: moker@uky.edu)

## ABSTRACT

The time of peak thermal conditions in the granulite facies zone of the southern Appalachian orogen corresponds to the time of formation of garnet-bearing leucosomes generated by biotite dehydration melting in garnet-sillimanite gneisses. Leucosomes contain unusually abundant zircon occurring as inclusions in euhedral plagioclase phenocrysts and garnet. Isotope dilution thermal-ionization mass spectrometric analysis of 13 elongate, euhedral zircon crystals from the leucosome yields a concordant U-Pb age of  $458 \pm 1.0$  Ma (MSWD = 0.095). Ion microprobe U-Pb analysis of 11 euhedral zircons yields a weighted age of  $460 \pm 12$  Ma ( $2\sigma$ ); 458 Ma is taken as the time of partial melting and peak thermal conditions attending melting. Only two of 39 leucosome zircons exhibit Proterozoic inheritance typical of most zircons in metapelitic rocks and granitic intrusions in the southern Blue Ridge. Mineralogic thermobarometry, oxygen isotope thermometry, and experimental studies constrain melting to have occurred at  $\sim 850^\circ\text{C}$  and 8 kbar. The garnet-rich leucosomes are unfoliated, crosscut the dominant regional fabric in sillimanite gneisses, and contain kyanite as a late or subsolidus phase. Leucosome textures (euhedral plagioclase phenocrysts with interstitial quartz) and major and trace element concentrations (low  $\text{SiO}_2$  and  $\text{K}_2\text{O}$ , high Zr) suggest that the leucosomes are not primary melts; they appear to be plagioclase-rich cumulates remaining after fractionation of a more felsic melt component. The Zr concentration of the leucosome is excessively high (1500–4000 ppm) for melts with compositions equivalent to the leucosome. The Zr enrichment in the leucosome resulted primarily from physical concentration of zircon by inclusion in plagioclase and garnet that remained after loss of the felsic component of the melt.

**Online enhancement:** table.

## Introduction

The southern Appalachian orogen is a complex amalgamation of terranes assembled during multiple periods of Paleozoic orogenesis. It has been proposed that the oldest major event, the Taconian orogeny, involved collision of Laurentia with the Piedmont/Jefferson terrane (Hatcher 1987; Horton et al. 1989). Although the metamorphic expression of this event is mid- to Late Ordovician in age (e.g., Butler 1972; Dallmeyer 1975; Glover et al. 1983; Kish 1991; Connelly and Dallmeyer 1993; Miller et

al. 1998), precise and reliable ages that can be directly correlated with specific metamorphic or deformational events or with deposition of Taconian clastic deposits in the foreland are rare. One exception is the precise age of eclogite facies metamorphism ( $458 \pm 1$  Ma) that has recently been documented in western North Carolina (Miller et al. 2000a). It is necessary to determine the exact timing of the collision-driven metamorphism in order to correlate the timing of this event in the southern Appalachians with Taconian orogenesis elsewhere in Laurentia.

This study addresses the regional tectonometamorphic question of timing of Taconian orogenesis in the southern Appalachians and the broader problem of correlating a radiometric age with a specific geologic event. Zircons that unequivocally nucle-

Manuscript received June 3, 2003; accepted October 25, 2003.

<sup>1</sup> Syracuse University, Department of Earth Sciences, Syracuse, New York 13244, U.S.A.; e-mail: sdsamson@mailbox.syr.edu.

<sup>2</sup> Vanderbilt University, Department of Geology, Nashville, Tennessee 37235, U.S.A.; e-mail: millercf@ctrvax.vanderbilt.edu.

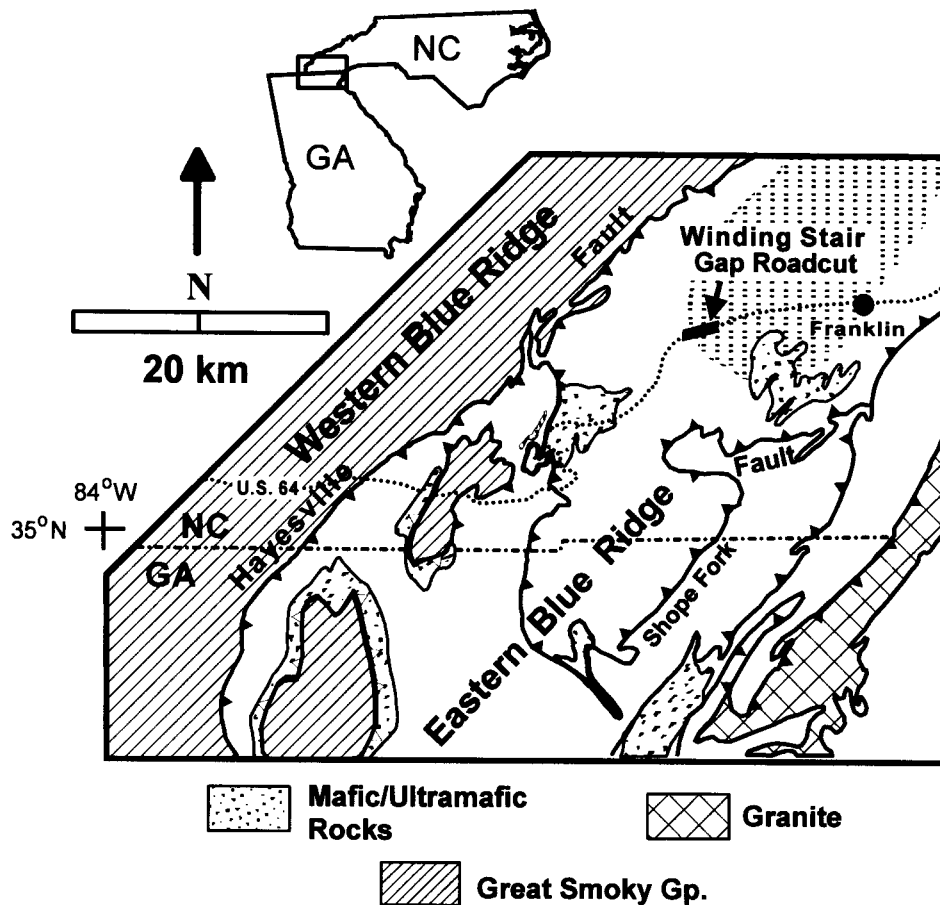


**Figure 1.** Location of the Winding Stair Gap road cut along U.S. Hwy 64 (dotted line) in the eastern Blue Ridge Province, southwestern North Carolina. Unpatterned area of eastern Blue Ridge is primarily high-grade semipelitic gneiss.

ated and grew (i.e., they are not inherited xenocrysts) in garnet-plagioclase leucosomes that crosscut the youngest foliation in the granulite facies gneisses of the southern Blue Ridge were used to determine the time of peak granulite facies metamorphism and resultant melting. Garnet-sillimanite gneisses, which are crosscut by and locally melt to form the leucosomes, are used to determine peak granulite facies pressure (P)-temperature (T) conditions using conventional cation-exchange and net-transfer reaction geothermobarometry. The leucosome crystallization temperature is further constrained by oxygen isotope exchange thermometry for leucosome and gneiss. A relatively precise P-T-time (t) point, in which P and T were established at a specific time t, is obtained in this manner. The unusually high abundance of zircon (and concentration of Zr in the leucosome) also warrants consideration of the behavior of zircon during high-grade metamorphism and melting. The majority of

the mass of zircon in the leucosome can be demonstrated to have crystallized from a melt and concentrated in the leucosome rather than being new growth nucleated on inherited cores or recrystallized zircon formed during high-grade metamorphism. The U-Pb age of zircon unequivocally corresponds to the time of generation of a melt phase that was preceded by granulite facies metamorphism.

#### Study Area

Samples of migmatitic gneiss were collected at the Winding Stair Gap (WSG) road cut in western North Carolina, located on the southern margin of the zone of granulite facies metamorphism in the eastern Blue Ridge (fig. 1; Hatcher and Butler 1979; Absher and McSween 1985; Eckert et al. 1989). Metapelitic lithologies typically contain biotite + plagioclase + garnet + quartz + sillimanite ± kya-

nite; kyanite can be shown to have formed after sillimanite (Moecher 1999). Muscovite is absent from all peak assemblages in the outcrop but occurs locally, having formed by retrograde rehydration reactions (Spear et al. 1999). Mafic units in this area contain orthopyroxene + clinopyroxene + garnet + hornblende + plagioclase (Eckert et al. 1989), consistent with the high-grade assemblages present at WSG.

Migmatitic gray gneiss is the dominant lithology in the road cut. At least two generations of leucosomes are present in outcrop. An early folded generation contains K-feldspar + plagioclase + quartz + biotite + garnet + rutile and was likely formed by an early phase of muscovite dehydration melting of quartz-bearing pelitic gneiss. The garnet- and plagioclase-rich leucosomes studied here are the youngest generation. These leucosomes crosscut the following structural elements: (1) the predominant foliation ( $S_1$ ; strike 040, dip 18°NW) defined by compositional banding in the gneiss (fig. 2, insets 3, 4); (2) a lineation (9° plunge bearing 295) defined by preferred orientation of the long axis of

acicular sillimanite; (3) the orientation of earlier leucosomes, which are folded about axes parallel to the sillimanite lineation; (4) the axial planes of folded early leucosomes; and (5) the orientation of calc-silicate lenses and boudins aligned parallel to the compositional layering in the migmatites. "Gneiss" as used here refers to the light gray plagioclase-biotite-garnet-sillimanite component of the migmatite evident in figure 2. The  $SiO_2$ -poor,  $Al_2O_3$ -rich bulk composition of this lithology may have been an original sedimentary feature, or (as we propose) it results from a previous period of melting that depleted it of quartz, muscovite, and some biotite (Patiño Douce and Johnston 1991). Details of the melting history of this sample and migmatites throughout the outcrop are the topic of future research.

### Methods

Isotope dilution thermal-ionization mass spectrometric (ID-TIMS) U-Pb analysis was carried out at Syracuse University on elongate, prismatic, doubly

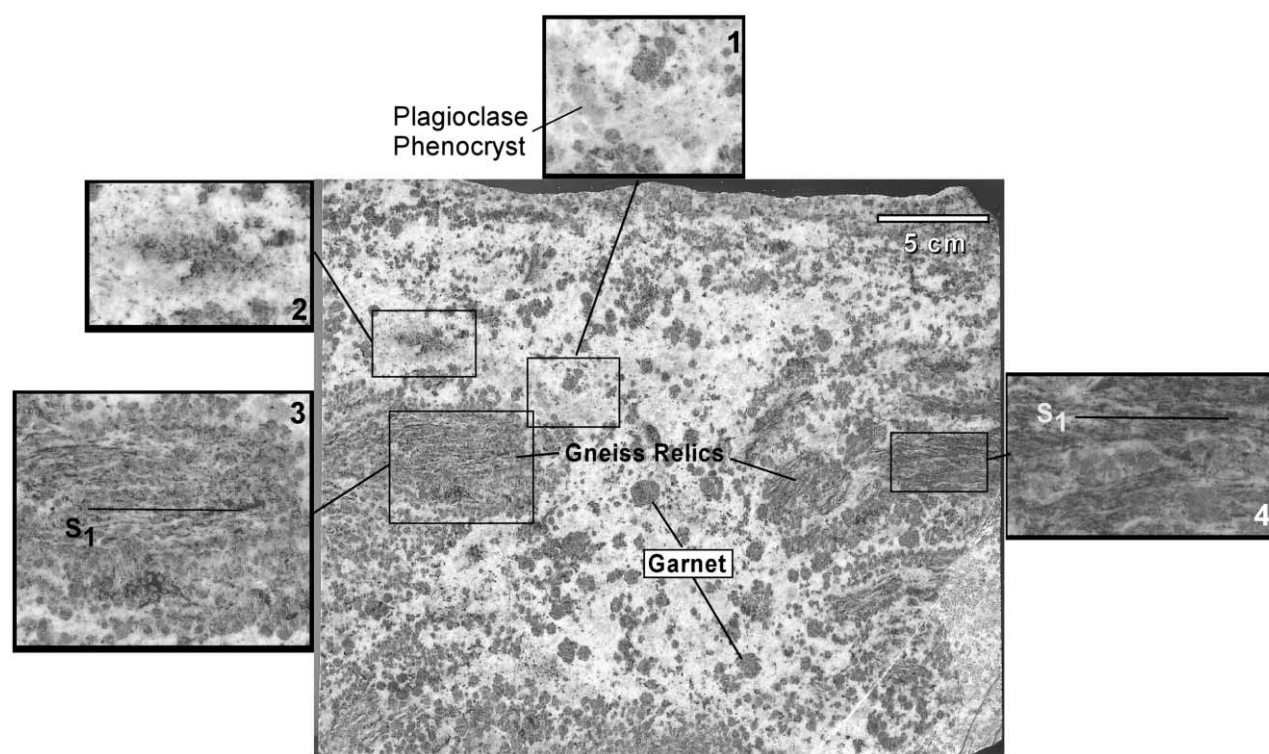


**Figure 2.** Sawed slab of migmatitic gneiss illustrating the typical relationship between garnet-rich leucosomes (*light-colored, hourglass-shaped area in center*) and relic fragments of biotite + sillimanite + garnet gneiss (*dark gray*). Inset 1 shows light gray plagioclase phenocrysts surrounded by white, finer-grained plagioclase. Inset 2 is a relic fragment of gneiss melting (assimilating?) into the leucosome. Insets 3 and 4 are enlargements of areas of gneiss showing foliation defined by parallelism of trains of garnet and parallel-aligned sillimanite needles.  $S_1$  = predominant foliation.

terminated zircons handpicked from a crushed thin section chip cut from the leucosome in the slab shown in figure 2. Four batches of zircon (a single xenocryst; two groups of five and one group of three crystals) were heavily abraded before analysis. Details of dissolution, chemical separation, and mass spectrometric protocols are given by Samson and D'Lemos (1998).

An additional set of the elongate, euhedral zircons similar to those used for TIMS analysis were handpicked for ion microprobe analysis. High-resolution ion microprobe U-Pb isotope data were acquired using the Cameca ims 1270 at UCLA and the Stanford/USGS SHRIMP-RG. Methods at UCLA were as described by Miller et al. (2000*b*), except that zircons were analyzed in situ in the thin section shown in figure 3*a*. The thin section was cut from the chip before the crushing and hand-

picking of the zircon. Stanford/USGS methods followed those of Bindeman et al. (2002), except that standard R33 (419 Ma) was used. The latter methods were used to analyze a suite of zircons identical to those used for ID-TIMS analysis.

Zoning in zircons was examined by back-scattered electron (BSE) and cathodoluminescence (CL) imaging to identify cores and distinguish magmatic from metamorphic growth zones (Carrigan et al. 2003; Ownby et al. 2004). Electron probe wavelength dispersive spectrometry microanalysis of garnet, biotite, and plagioclase for the purposes of conventional geologic thermobarometry was carried out at the University of Kentucky on an ARL SEMQ instrument. Multiple analyses were made of biotite and plagioclase to assess homogeneity within a thin section, and compositional traverses of all garnets were made to assess the extent of

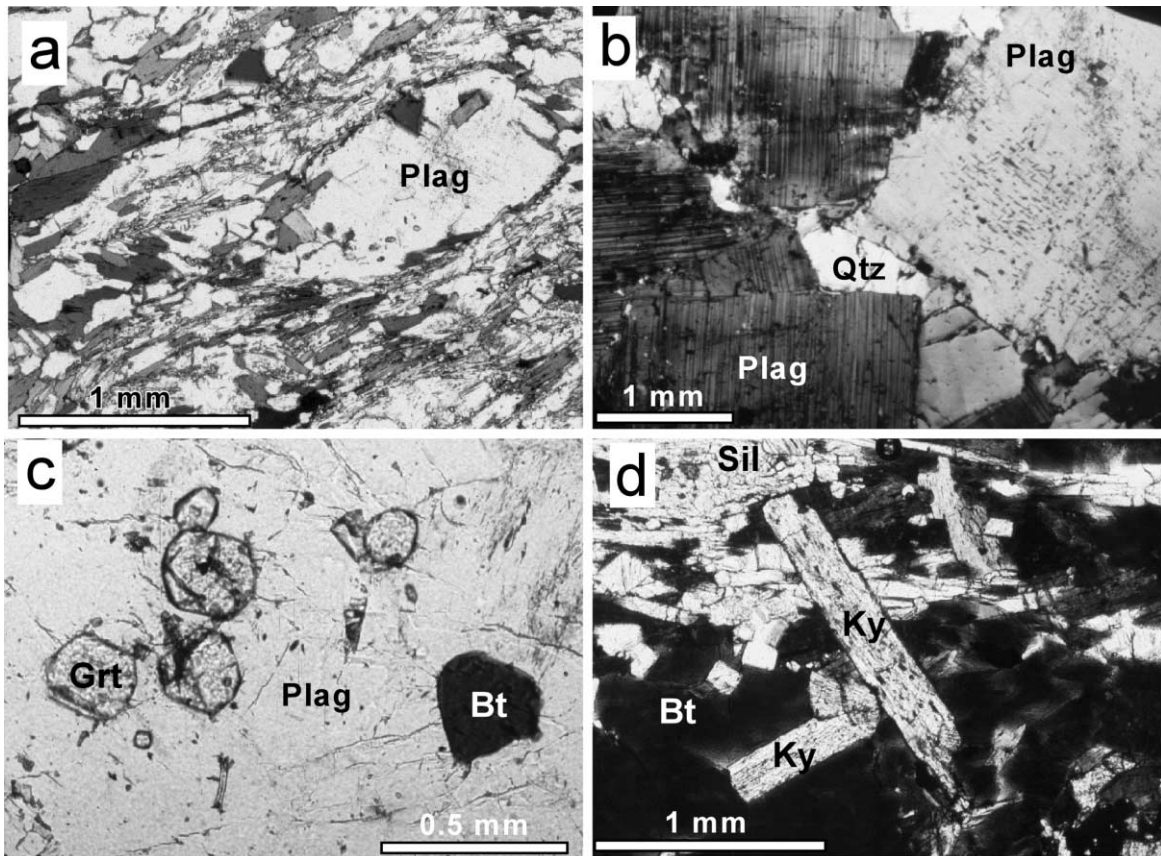


**Figure 3.** Photomicrographs illustrating petrologic characteristics of the gneiss. *a*, Matrix of biotite-sillimanite (high relief needles)-plagioclase (*Plag*) gneiss; main matrix foliation (*S<sub>1</sub>*) trends diagonally from upper right to lower left. *b*, Sub- to euhedral phenocrysts of plagioclase in leucosome with interstitial quartz (*Qtz*). Dark inclusions within plagioclase at upper right are K-feldspar. *c*, Inclusions of garnet (*Grt*) and biotite (*Bt*) in plagioclase in gneiss. *d*, Temporally late, coarse-grained kyanite (*Ky*) growing across horizontal foliation defined by biotite and sillimanite (*Sil*) in gneiss.

**Table 1.** Major (wt%) and Trace Element (ppm) Contents of Migmatite Components

	C-G	K-G	E-L	G-L	H-L	Melt
SiO <sub>2</sub>	45.55	46.63	52.25	53.87	52.26	65.5
TiO <sub>2</sub>	1.11	1.06	1.25	1.18	1.06	.3
Al <sub>23</sub>	24.96	24.62	22.84	23.57	22.67	17.1
Fe <sub>2</sub> O <sub>3</sub>	15.23	14.08	9.29	5.25	9.99	9.1
MnO	.46	.38	.29	.15	.31	.1
MgO	4.53	3.92	2.61	1.43	2.73	.73
CaO	4.10	4.31	5.43	6.37	5.24	3.35
Na <sub>2</sub> O	2.61	3.07	4.53	5.12	4.08	2.39
K <sub>2</sub> O	.76	1.05	.57	.71	.57	2.08
P <sub>2</sub> O <sub>5</sub>	.11	.11	.08	.06	.08	
LOI	-.08	.23	.12	.28	.17	
Total	99.32	99.46	99.27	97.99	99.17	
Pb	18.5	11.5	14.2	18.5	11	
Nb	77.6	96.9	223.8	189.2	167.5	
Zr	249.7	373.2	1521.7	4008.3	1858.5	
Y	104.1	114.9	106	48.5	112	
Sr	527.6	525.5	761.2	963.4	738.1	
Rb	19.4	23.6	3.3	3.7	3.7	
Ga	41	34.9	27.1	29.3	27.5	
Zn	112.6	108.4	48.6	35.4	53.6	
Ni	71.7	52	6.5	14.4	23.8	
Ba	455.3	565.5	210.6	296.7	251.0	
Co	59.1	54.6	30.8	40.3	38.6	
V	111.7	101.2	44	34.8	49	
T <sub>zs</sub> (°C) <sup>a</sup>	850	879	1009	1128	1046	
Zr <sup>b</sup>			365	410	338	247

Note. Major and trace element contents were determined by XRF at Washington University, St. Louis. See article by Couture et al. (1993) for analytical details. G = chip cut from slab in figure 2 that is mostly Bt-Grt-Sil-Pl gneiss; L = chip cut from slab that is garnet-plagioclase leucosome. Melt composition was derived from gneiss calculated using method of Winther (1996).

<sup>a</sup> Zircon saturation temperature for melt with composition of the whole rock (Watson and Harrison 1983).

<sup>b</sup> Calculated equilibrium Zr concentration in zircon-saturated melt with composition of the whole rock at 850°C.

retrograde zoning and determine inferred peak compositions. Qualitative x-ray maps were made of selected garnets to assess the spatial pattern of any zoning. The P-T conditions attending granulite facies metamorphism and melting were calculated from the intersection of the P-T locus of the garnet-biotite (GARb) Fe-Mg exchange and garnet-aluminosilicate-quartz-plagioclase (GASP) net transfer equilibria using the computer program TWQ (Berman 1991). In order to mitigate the effects of retrograde Fe-Mg exchange between garnet and biotite (e.g., Spear and Florence 1992), we analyzed biotite grains and in some cases garnet porphyroblasts that occur as inclusions in plagioclase (fig. 3c). Such biotites generally contain higher Fe/(Fe + Mg) and Ti contents than do biotites located at grain boundaries. These are interpreted to represent the peak biotite compositions because this textural variety of biotite was insulated from retrograde Fe-Mg exchange with modally dominant garnet. In that garnet and sillimanite also occur as inclusions in plagioclase in many samples, we feel confident that biotite had equilibrated with garnet that is being used in the P-T calculations. The agreement of the temperatures obtained from conventional ther-

mobarometry with those obtained from oxygen isotope fractionations between K-feldspar and garnet and sillimanite in metapelites from the same outcrop provides corroborating support for this approach. Multiple garnet core, biotite inclusion, and matrix plagioclase compositions were obtained for 12 samples of gneiss and leucosome.

Whole-rock major and trace element x-ray fluorescence (XRF) analyses were obtained on five selected areas of the leucosome and gneiss. These analyses permitted calculation of zirconium saturation temperatures and comparison of gneiss and leucosome compositions. Five rock chips, each approximately 10–15 cm<sup>3</sup> in volume, were sawed from the matching face of the slab of migmatite shown in figure 2. Three of the chips are garnet-plagioclase leucosome, and two are primarily gneiss with minor leucosome. Major and selected trace element abundances obtained by XRF spectrometry are compiled in table 1. Finally, selected trace element concentrations (Zr, Ti, Cr, Y, rare earth element [REE]) were measured by laser ablation indirectly coupled plasma mass spectrometry (LA-ICP-MS) on two garnets (I. Ridley and E. Haynes, pers. comm., 2002). Garnet tends to par-

tition Zr relative to most minerals (except hornblende; Fraser et al. 1997); the modally abundant garnet may therefore contribute to the Zr budget of the leucosome.

Oxygen isotope analyses of garnet and plagioclase from the leucosome were carried out at the University of New Mexico following the laser heating method of Sharp (1995). Additional details of isotopic analysis are presented by Moecher and Sharp (1999).

### Sample Characterization

**Mineralogy and Textural Relationships.** The textural and mineralogic features are relevant to interpretation of the origin of the leucosomes and to geothermobarometry and geochronometry. Absher and McSween (1985) present a complete description of the various lithologies exposed in the road cut.

Figure 2 shows a slab of the migmatitic gneiss with typical garnet-bearing leucosome; this slab matches that from which all zircons were extracted. The leucosome crosscuts the faint relict foliation defined by a compositional layering and sillimanite lineation in the gneiss (fig. 2, *insets* 3, 4). Several relict gray patches of gneiss ranging down to 1 cm across can be seen to fade gradually into leucosome (fig. 2, *inset* 2). The gneissic domains consist of plagioclase + biotite + sillimanite + garnet + rutile (fig. 3a); quartz was not found in any thin sections of gneiss cut from the slab. The leucosome clearly crosscuts the weak foliation and sillimanite lineation in the gneiss. Boudinage of layers of pelitic and calc-silicate gneiss, with envelopment of boudins by leucosomes, is a common feature throughout the road cut.

The leucosome consists primarily of medium- to coarse-grained plagioclase, which occurs as anhedral, equant grains and locally of euhedral phenocrysts, with rare quartz occupying the interstices among the latter (fig. 3b). The plagioclase is commonly antiperthitic (fig. 3b) and may contain inclusions of biotite, small (100–500  $\mu\text{m}$ ) garnets, zircon, or sillimanite (fig. 3c). Some plagioclase exhibits combined Carlsbad and albite twinning.

Garnet porphyroblasts comprise a major modal component of the gneissic relicts (fig. 2, *inset* 3) and are typically finer grained (1–3 mm) than the 5-mm- to nearly 1-cm-diameter grains in the leucosome. The garnet is locally concentrated in planar arrays within and adjacent to gneiss relicts (fig. 2). Garnet in the leucosome is more spherical compared with ellipsoidal garnet within gneiss (fig. 2, *inset* 4). Inclusions in gneissic and leucosome gar-

net consist of plagioclase, rutile, biotite, sillimanite, and zircon. Sillimanite inclusions in garnet are generally finer grained than those in the matrix and often show a preferred alignment or are concentrated in a circular band in the garnet. Leucosome garnet contains crystallographically oriented acicular needles that BSE examination and energy dispersive spectrometry analysis reveal to be rutile. The coarsest garnets exhibit a subtle zonation of these inclusions.

Biotite comprises 10–20 modal percent of the gneiss, a sufficient amount to impart a light gray cast in hand sample compared with the nearly white leucosomes (fig. 2). Biotite in the gneiss defines a weak foliation expressed by a crystallographically preferred orientation of the (001) plane that anastomoses around plagioclase grains (fig. 3a).

Sillimanite is by far the dominant aluminosilicate polymorph in the gneissic relicts among the leucosome (and in rocks throughout the outcrop), occurring as bundles of acicular to bladed grains or as inclusions in plagioclase and garnet. Kyanite is rare but present in the leucosome. Kyanite abundance elsewhere in the road cut is higher in more biotite-rich schistose rocks, growing across the foliation defined by biotite and the lineation defined by sillimanite (fig. 3d).

Zircon in the leucosome occurs as clusters of equant crystals in plagioclase grains; along plagioclase or garnet grain boundaries; included in garnet (fig. 4a, 4b); or as individual, elongate, euhedral crystals included in plagioclase (fig. 4c). The equant zircons exhibit, in BSE images, weakly zoned cores with unzoned margins (fig. 4d). The elongate zircons exhibit, in CL images, a concentric zoning pattern that mimics the outline of the crystal faces (fig. 4e). These zoning patterns contrast with those from Sil-Grt-Bt-Pl gneiss elsewhere in the road cut, which tend to have oscillatory zoned, variably resorbed cores that are clearly inherited (detrital) and are overgrown by unzoned rims interpreted to be metamorphic (fig. 4f; Miller et al. 1998).

Zircon occurs within the gneiss but is not strikingly as abundant in gneiss as it is in the leucosome. The zircons in gneiss consist mainly of relatively small (20  $\mu\text{m}$ ) equant grains, the most conspicuous of which are those included in biotite as revealed by pleochroic haloes.

**Whole-Rock Chemistry.** Leucosomes are relatively low in Si and K and high in Al, Fe, Ca, and Na (table 1) compared with a typical felsic leucosome in migmatites interpreted to form by dehydration melting of a quartz- and biotite-bearing metapelite (e.g., Patiño Douce and Johnston 1991; Vielzeuf and Montel 1994; Gardien et al. 1995; Pa-

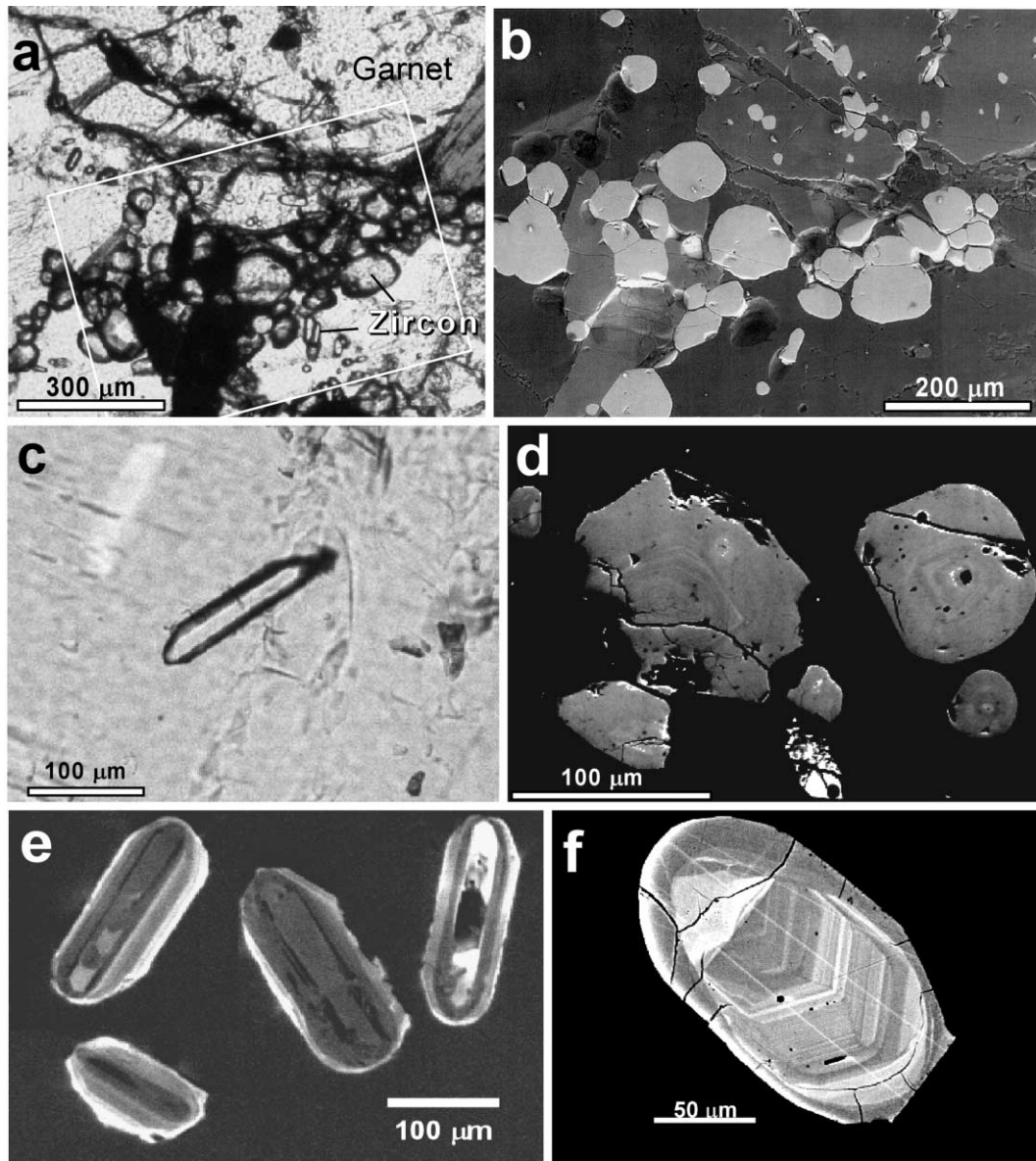


**Figure 4.** Photo- and electron micrographs of zircon and leucosome textures. *a*, Plane light photomicrograph and *(b)* back-scattered electron (BSE) image of area outlined in *a* showing abundant equant to elongate zircons and their relationship to garnet in the leucosomes (*lightest gray* = zircon, *medium gray* = garnet, *darkest gray* = plagioclase). *c*, Plane light photomicrograph of elongate zircon included in plagioclase, representative of zircon picked for U-Pb TIMS and second session of ion microprobe analysis. *d*, BSE image of faintly zoned equant zircons in same thin section as sample shown in *a* and *b* used for initial U-Pb ion microprobe age determinations by Moecher and Miller (2000). *e*, Cathodoluminescence image illustrating zoning pattern in elongate zircons picked for TIMS and ion microprobe analysis. *f*, BSE image of zircon showing oscillatory-zoned, inherited core with unzoned metamorphic rim, representative of zircons in gneiss from elsewhere in the Winding Stair Gap outcrop (Miller et al. 1998).

tiño Douce and Beard 1995). Leucosome chemistry reflects the garnet- and plagioclase-rich and K-feldspar- and quartz-poor nature of the leucosome. By comparison, the gneiss is even more mafic and Al-rich than the leucosome with which it is in contact. The most striking characteristic of the leucosome

is the exceptionally high Zr content (1500–4000 ppm), which contrasts with the lower Zr in the gneiss (250–370 ppm) that is more typical of that in high-grade pelitic or granitic rocks (Fraser et al. 1997). Calculated equilibrium concentrations of Zr for zircon-saturated melts with major element

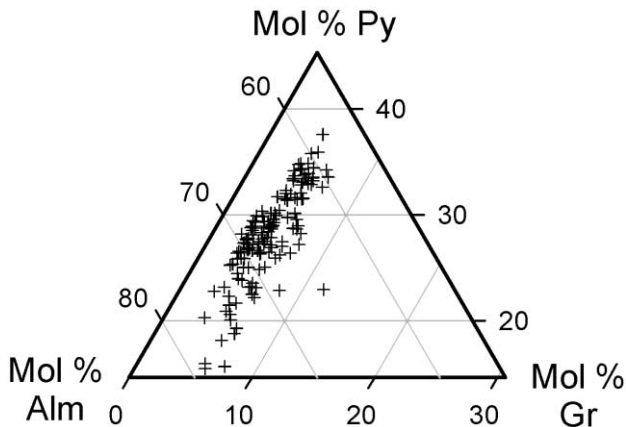


**Figure 5.** Ternary diagram illustrating range of garnet compositions from gneiss and leucosome.

compositions equivalent to the leucosomes are 340–410 ppm (table 1). The high concentrations of Al, Fe, Mg, Y, Nb, and Sr and the low concentrations of Si, K, and Rb in the gneiss suggest that it is a restite the presently observed episode of biotite dehydration melting and potentially an earlier episode of dehydration melting involving muscovite (Le Breton and Thompson 1988; Patiño Deuce and Johnston 1991; Gardien et al. 1995).

**Mineral Chemistry.** Garnets in gneiss and leucosome are Fe-Mg solid solutions with relatively high Mg, reflecting the high metamorphic grade, and with minor Ca and Mn (table 2, available in the online edition of the *Journal of Geology* and also available from the *Journal's* Data Depository in the *Journal of Geology* office upon request; fig. 5). Garnet compositions in high-grade rocks typically vary because of bulk rock composition or variable degrees of postpeak T diffusional resetting, the extent of which in a specific porphyroblast is controlled by size, cation diffusion rates, and cooling rate. Most garnets analyzed here are compositionally homogeneous with regard to the major components, except within 50  $\mu\text{m}$  of rims, consistent with equilibration of garnets at high temperature with minor diffusional rim exchange (fig. 6). A typical garnet core composition is  $X_{\text{Fe}} = 0.63$ ,  $X_{\text{Mg}} = 0.31$ ,  $X_{\text{Mn}} = 0.02$ ,  $X_{\text{Ca}} = 0.04$  (table 1; fig. 7). However, the coarsest garnet examined, which is a  $\sim 5$ -mm-diameter garnet in the leucosome, exhibits a high Ca core ( $X_{\text{Ca}} = 0.12$ ; table 1; figs. 7, 8). This high Ca core is a diffuse oval region (Ca x-ray map, fig. 8) that corresponds spatially with the rutile inclusions described above. This core is a relict growth feature from early stages of garnet growth on initial stages of melting that did not chemically

homogenize during the time over which the rocks were at high temperature.

The Zr concentration in garnet is only  $\sim 10$  ppm on the basis of LA-ICP-MS analysis of two coarse-grained garnet porphyroblasts in the leucosome (I. Ridley, pers. comm.; one such garnet is shown in fig. 8). This concentration is relatively low compared with measured Zr concentrations in garnet from granulites (e.g., 20–50 ppm Zr; Fraser et al. 1997) and calculated equilibrium Zr concentrations expected for garnet coexisting with zircon and quartz at 800°–900°C (40–150 ppm; Donahue et al. 2001). Although modally abundant, garnet does not contain sufficient Zr to affect the Zr budget of the melt-forming process.

The greatest proportion of plagioclase grains from gneiss and leucosome range in composition from An 34 to An 46 (table 2; fig. 9). Exceptions are relatively calcic plagioclase ( $\sim$ An 50) from a plagioclase-biotite-garnet gneiss also containing hercynite and corundum and sodic plagioclase ( $\sim$ An 25) in a biotite- and sillimanite-rich gneiss not associated with the leucosome. These extreme compositions are bulk compositional effects. Plagioclase from the leucosome has the same composition as that in gneiss (fig. 9). Plagioclase is generally unzoned chemically and contains minor amounts of  $\text{K}_2\text{O}$ . The alkali feldspar inclusions in antiperthitic plagioclase contain approximately 6 mole % albite component.

Biotite is an intermediate Fe-Mg solid solution with high Ti contents; the highest  $\text{TiO}_2$  in each

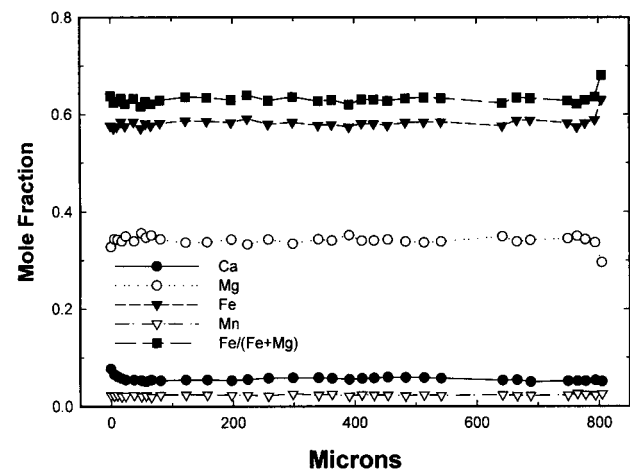


**Figure 6.** Chemical variation within a fine-grained garnet in leucosome. Note flat profile across the core and minor variation at margins resulting from retrograde Fe-Mg exchange with biotite and minor resorption of garnet rim.

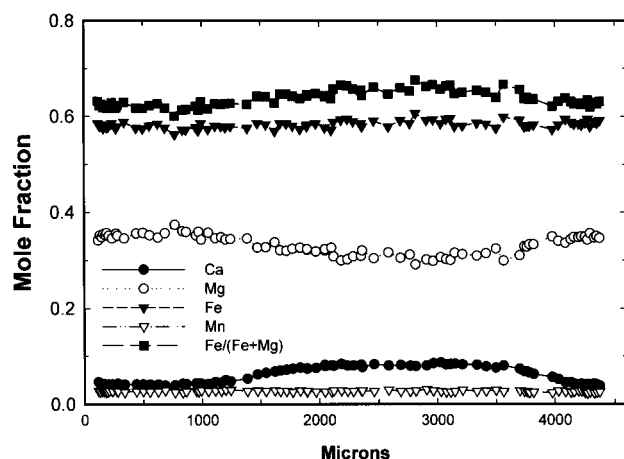


**Figure 7.** Chemical variation across a single coarse-grained garnet porphyroblast from the leucosome. The compositional variation is inferred to result from early growth of high Ca garnet in initial stages of biotite dehydration melt reaction, overgrown by a lower Ca rim.

sample ranges from 4.2 to 5.2 wt%, the latter corresponding to 10% of the octahedral site in biotite (table 2). Biotite ranges by 10 mole % in terms of Fe/(Fe + Mg) in individual samples. The high Ti contents are consistent with the high T biotites produced in partial melting experiments on meta-graywacke and metapelite at temperatures of  $900^{\circ} \pm 75^{\circ}\text{C}$  (Patiño Douce et al. 1993; Patiño Douce and Beard 1995).

## Results

**Geochronometry.** Three batches of zircons analyzed by U-Pb TIMS (table 3) are concordant and in excellent agreement, yielding a mean  $^{238}\text{U}/^{206}\text{Pb}$  date of  $458 \pm 1.0$  Ma (MSWD = 0.095; fig. 10a). A fourth analysis of a single zircon crystal was discordant, yielding a  $^{207}\text{Pb}/^{206}\text{Pb}$  date of 805 Ma. A regression line through this point and 458 Ma intersects concordia at 1068 Ma, a common date for xenocrystic zircon cores in the area (Miller et al. 1998).

A total of 48 spot analyses were performed by ion microprobe, 34 at UCLA (17 each of cores and rims in a thin section) and 14 at Stanford (from a hand-picked separate; mostly interiors, but the ion beam generally overlapped the rim). In BSE and CL images, almost all grains have a small, distinct, zoned core and a thick, weakly zoned to unzoned rim (fig. 3c). The cores are centered in the grains, are nearly equant to strongly elongated (aspect ratio  $\sim 1$  to  $\sim 8$ ), and have euhedral zoning that is not truncated by

the rim zone. Grains appear rounded (weakly faceted). The grains in the thin section are  $<10$  to near  $100 \mu\text{m}$  in maximum dimension and are included within garnet, plagioclase, and biotite; only grains  $>20 \mu\text{m}$  were analyzed (spot size was  $\sim 10 \mu\text{m}$ ). Most grains in the thin section are nearly equant. Grains from the separate analyzed at Stanford are larger and generally more elongate (typically  $\sim 200 \mu\text{m} \times 100 \mu\text{m}$ ). A single grain from the mineral separate has an unusually large, unzoned bright (in CL) core, but otherwise, zoning is similar.

The 34 analyses from the thin section collected at UCLA cluster at 470 Ma ( $470 \pm 5$  Ma [ $2\sigma$ ], MSWD = 0.8; fig. 10b). Core and rim dates are indistinguishable. Eleven analyses collected at Stanford yield a pooled date of  $460 \pm 12$  Ma ( $2\sigma$ , MSWD = 0.9); two dates of slightly less than 400 Ma probably reflect Pb loss and were omitted. The large core analyzed at Stanford has a  $^{238}\text{U}/^{206}\text{Pb}$  date of 1.20 Ga. We are uncertain whether the apparent differences in age between the UCLA analyses of grains in thin section and the Stanford analyses of separated grains (and the TIMS results) are real or reflect different analytical conditions. We tentatively suspect the latter and emphasize that in any case, all three independent analytical efforts yield a Middle to Late Ordovician age.

The closure temperature for Pb diffusion in zircon (in excess of  $900^{\circ}\text{C}$ , depending on grain size and cooling rate; Cherniak and Watson 2001) exceeds the peak temperature attending melting. This is consistent with our interpretation that the zircon date corresponds to the time of zircon growth and not cooling from peak conditions.

**P-T Conditions.** Figure 11 is a compilation of all GARB and GASP thermobarometric calculations using garnet cores and biotite inclusions in K-feldspar and plagioclase for 10 samples of sillimanite

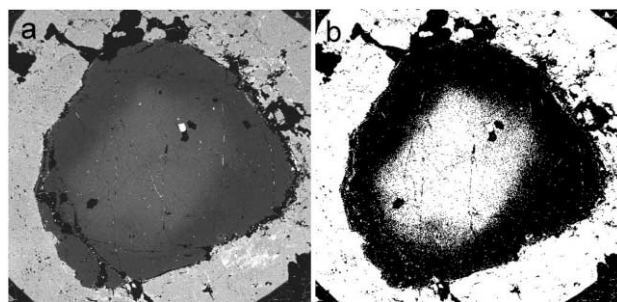


**Figure 8.** Two-dimensional variation in Ca concentration for coarse-grained garnet in figure 7, depicted in gray scale (a) and threshold x-ray mode (b) to emphasize the compositional difference between core and rim.

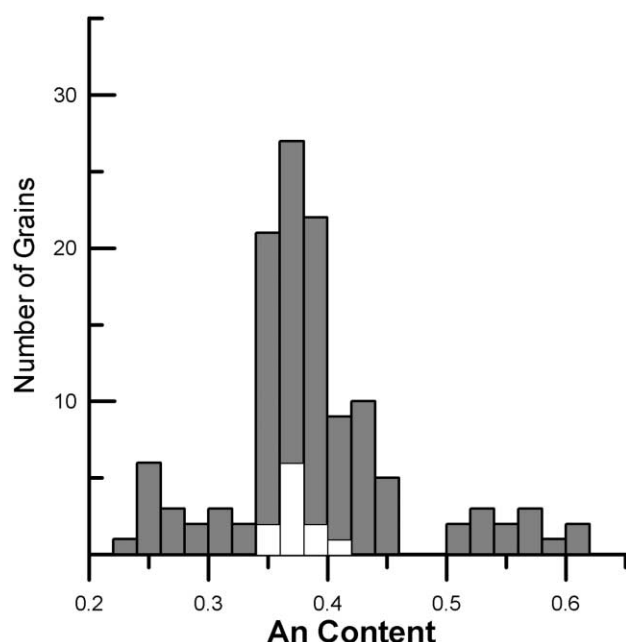


**Figure 9.** Histogram illustrating compositional range of plagioclase from samples of gneiss collected throughout the outcrop (gray) and leucosome shown in figure 2 (white).

gneiss in the outcrop containing the leucosome. The P-T region of intersection of GARB and GASP is  $850^{\circ} \pm 40^{\circ}\text{C}$  at 7–9 kbar. Also shown are the constraints from oxygen isotope thermometry. The difference between plagioclase and garnet oxygen isotope compositions ( $\Delta^{18}\text{O}_{\text{Pl-Grt}}$ ), obtained on minerals separated from the same chip of leucosome used to extract zircon for geochronology, is  $1.33 \pm 0.26$  per mil ( $\delta^{18}\text{O}_{\text{SMOW}} = 8.36$  and  $7.02$  per mil for Pl and Grt, respectively, which corresponds to a T of  $880^{\circ} \pm 100^{\circ}\text{C}$ ; Qtz-Grt fractionation of Sharp [1995]; Qtz-Pl fractionation of Bottinga and Javoy [1973]). The temperature precision is low because of the relatively small fractionation of  $^{16}\text{O}$  and  $^{18}\text{O}$  between plagioclase and garnet. The high closure temperature for oxygen diffusion in garnet and the high modal abundance of plagioclase preclude significant resetting of mineral oxygen isotope compositions and favor retention of a high-temperature fractionation (Giletti 1986; Eiler et al. 1993; Farquhar et al. 1993). K-feldspar-garnet and K-feldspar-sillimanite oxygen isotope fractionations for a sample of Bt-Sil-Grt-Kfs gneiss from elsewhere in the outcrop, also used for conventional thermobarometry (93–1; table 1), yield temperatures of  $840^{\circ}$  and  $850^{\circ}\text{C}$ , respectively (Moecher and Sharp 1999), corroborating the relatively high T determined by

mineral equilibria for the gneiss and oxygen isotope compositions for the leucosome. Although we have applied relatively robust approaches for geothermometry, all the thermometric systems are susceptible to retrograde exchange on cooling, and temperatures may be minimum estimates of temperatures attending granulite facies metamorphism and melting.

The conventional and stable isotopic temperatures determined here are consistent with experimentally determined conditions for biotite dehydration melting reactions in pelitic bulk compositions at approximately 5–10 kbar ( $850^{\circ}$ – $900^{\circ}\text{C}$ ; Vielzeuf and Holloway 1988; Patiño Douce and Johnston 1991; Vielzeuf and Montel 1994; Carlington and Harley 1995; Gardien et al. 1995). In view of the extensive Ti and Fe-Mg solid solution in biotite and Ca-Na solid solution in plagioclase, melting probably occurred over a range of temperature during prograde heating.

## Discussion

**Interpretation and Relevance of Dates.** The date for metamorphism/melting obtained here is the youngest and most precise date determined thus far for the time of Taconian metamorphism in the southern Blue Ridge Province. Miller et al. (1998) obtained a pooled metamorphic U-Pb ion probe date of  $495 \pm 14$  Ma ( $2\sigma$ ) for metamorphic zircon rims in pelitic gneiss at WSG. Leucosome was carefully excluded from material from which these zircons were separated, and the grains invariably contained large Mesoproterozoic cores. Because these rims were extremely U-poor ( $\sim 10$ – $20$  ppm), analytical uncertainty for individual analyses was large, but they appear to define a population that is distinctly older than the leucosome zircons described here.

The precise time of Taconian orogenesis is poorly defined in crystalline rocks of the southern Blue Ridge, although we would expect there to be diachroneity along strike because the orogen is assembled from discrete terranes. Numerous K-Ar and  $^{40}\text{Ar}/^{39}\text{Ar}$  whole-rock and mineral (white mica in phyllites and slates; biotite, muscovite, hornblende) dates, in rocks of chlorite to upper amphibolite facies throughout southwestern North Carolina (summarized in Kish 1991), could be interpreted to correspond in the broadest sense to Taconian orogenesis. The metamorphic isograds that increase in intensity from northwest to southeast, approximately parallel to strike of the western Blue Ridge, across the Hayesville Fault and into the eastern Blue Ridge (i.e., the location of the present

**Table 3.** U-Pb Isotopic Data (TIMS) for Zircons from Winding Stair Gap

Analysis	Total U (ng)	Total Pb (pg)	Total common Pb (pg)	Atomic ratios								Ages (Ma)			$\rho^c$
				$\frac{^{206}\text{Pb}^a}{^{204}\text{Pb}}$	$\frac{^{206}\text{Pb}^b}{^{208}\text{Pb}}$	$\frac{^{206}\text{Pb}^b}{^{238}\text{U}}$	Error (%)	$\frac{^{207}\text{Pb}^b}{^{235}\text{U}}$	Error (%)	$\frac{^{207}\text{Pb}^b}{^{206}\text{Pb}}$	Error (%)	$\frac{^{206}\text{Pb}}{^{238}\text{U}}$	$\frac{^{207}\text{Pb}}{^{235}\text{U}}$	$\frac{^{207}\text{Pb}}{^{206}\text{Pb}}$	
				A (5)	1.32	95.2	.72	7529	11.72	.07353	.31	.5695	.33	.056173	
B (5)	.79	58.1	2.7	1319	9.32	.07361	.51	.5693	.54	.056091	.17	457.9	457.6	456.0	.951
C (3)	.58	42.3	1.2	2122	11.23	.07360	.36	.5698	.39	.056152	.13	457.8	457.9	458.4	.939
D (1)	1.05	111	.40	13,911	12.45	.10646	.11	.9683	.15	.065970	.098	652.2	687.6	805.4	.748

Note. All zircons were heavily abraded before analysis. Number of zircon crystals analyzed is given in parentheses.

<sup>a</sup> Measured ratio (uncorrected for fractionation, spike, or blank).

<sup>b</sup> Corrected for fractionation plus Daly bias ( $0.18\% \pm 0.09\% \text{ amu}^{-1}$ ), spike, blank, and initial Pb. Errors are  $2\sigma$ . Laboratory Pb blank ranged from 0.4 to 2 pg ( $\pm 50\%$ ) during the course of the study; U blank is  $\leq 0.5$  pg ( $\pm 50\%$ ). Initial common Pb composition is estimated using the crustal growth model of Stacey and Kramers (1975).

<sup>c</sup>  $^{207}\text{Pb}/^{235}\text{U}$ - $^{206}\text{Pb}/^{238}\text{U}$  error correlation coefficient (following Ludwig 1988).

study; isograds from Carpenter [1970] and Eckert et al. [1989]), imply a single phase of what has been assumed to be Taconian metamorphism. The U-Pb zircon date obtained here precisely confirms this assumption. However, a single phase of Taconian prograde metamorphism would be expected to be diachronous perpendicular to strike of the isograds, with the thermal peak and onset of cooling for successively higher grades occurring at later times (i.e., yielding younger dates) relative to the onset of crustal thickening associated with collisional orogenesis (Thompson and England 1984). With a judicious selection of geochronometers and taking into account variable diffusivities of daughter isotopes, we therefore expect rocks in the granulite facies zone of the southern Blue Ridge to yield the youngest ages for peak metamorphism compared with lower-grade rocks to the northwest in the WBR. Preliminary monazite U-Th-Pb chemical ages for Great Smoky Group metapelites, interpreted to represent the time of staurolite- and kyanite-grade metamorphism, are approximately 480 Ma (Moecher et al. 2003), consistent with this interpretation.

The zircon ages reported here agree with the proposed youngest limit for the time of the Taconian orogeny in the central Appalachians (458 Ma; Sinha 1997). This age is indistinguishable from that determined for eclogite facies metamorphism in the Spruce Pine Thrust Sheet of the eastern Blue Ridge, ca. 150 km along strike to the northeast (Miller et al. 2000a). The granulite facies metamorphism in metasediments of the EBR may correspond to that in an accretionary wedge paired with the subduction zone that resulted in eclogite facies metamorphism. The age corresponds biostratigraphically to the Llandeilian-Caradocian boundary (Tucker et al. 1990) and the youngest time of deposition in the Sevier foreland basin of eastern Tennessee. Thus, the final phase of metamorphism in accreting Ta-

conian terranes corresponds temporally to the waning of sedimentation in the foreland basin (Drake et al. 1989). Prograde metamorphism would correspond to progressive crustal thickening during the Blountian phase of Taconian orogenesis.

The prograde P-T path leading up to peak thermal conditions was through the sillimanite field, as indicated by the abundance of sillimanite in the gneissic protoliths throughout the outcrop. The presence of kyanite in the leucosome and evidence of kyanite forming after sillimanite in numerous samples of gneiss (fig. 3d; Moecher 1999) indicate that the P-T path evolved into the kyanite field as the rocks cooled from peak granulite-grade conditions. The petrologic evidence and high peak T/P support an anticlockwise P-T path that reached maximum thermal conditions at 458 Ma.

**Implications for Zircon Geochronometry.** This study demonstrates that growth of a phase used for geochronometric purposes (zircon) can be related to a specific tectonometamorphic event: melting attending granulite facies metamorphism, at peak T and probably peak P of the P-T path, the final event in a protracted Taconian orogenic cycle. Several recent studies have explored the behavior of zircon during high-grade metamorphism. In particular, these studies examine the relationship between zircon U-Pb ages and the time of peak thermal conditions, prograde reactions, and episodes of deformation and melting. In some cases, the zircon U-Pb age may correspond to the time of prograde reactions leading up to the thermal peak (e.g., Fraser et al. 1997), or it may represent the time of attainment of the thermal peak but not the peak pressure (Roberts and Finger 1997), the time of solid-state recrystallization of zircon in igneous protoliths of gneisses (Hoskin and Black 2000), or the time of a period of subsolidus annealing preceding or following peak thermal conditions (Schaltegger et al. 1999).

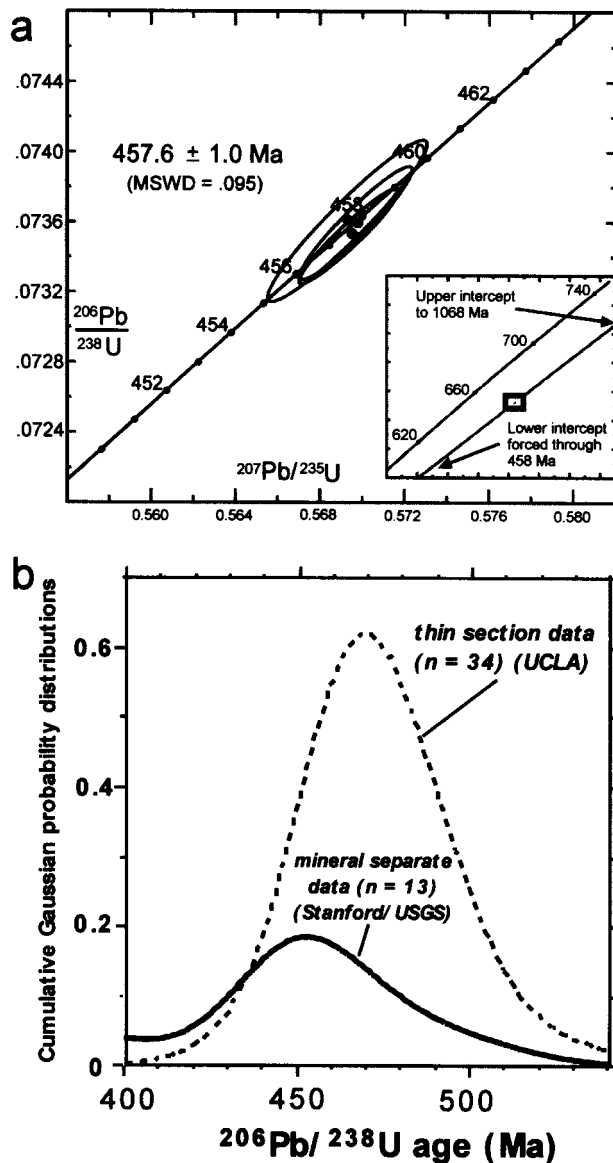
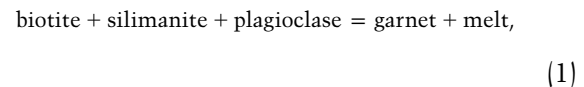


**Figure 10.** *a*, Concordia diagram for zircons analyzed by TIMS. The three analyses, consisting of two batches of five zircons and one batch of three zircons, overlap concordia and have a weighted mean  $^{238}\text{U}/^{206}\text{Pb}$  age of  $457.6 \pm 1.0$  Ma. *Inset*, Concordia diagram for a single equant xenocrystic zircon. *b*, Probability age distribution plot for two populations of euhedral zircons analyzed by ion microprobe.

Zircon is highly refractory, insoluble in various melt and fluid compositions, stable under weathering and sedimentary transport conditions (Watson and Harrison 1983; Watson 1996), and typically retains remnants of earlier growth histories. Thus, the present zircon occurrence and apparent mode of formation is particularly interesting. Very little

zircon from the parental metapelitic gneiss was physically entrained in extracted melt. Much of the initial zircon dissolved into the melt, with this dissolved zircon component eventually reprecipitating as 458 Ma magmatic crystals. The remainder, undissolved restitic zircon, was retained in the residual gneiss. Understanding the conditions and processes that essentially resulted in recycling of Zr has implications for zircon geochronology in general and for interpretation of the meaning of zircon ages in specific metamorphic terranes. Although additional detailed electron imaging, trace element analysis, and ion probe analysis of the various metamorphic phases in the WSG migmatites are necessary to fully explore these issues, we present some preliminary observations that serve as background for future work.

**Origin of Leucosomes.** The spatial association of leucosome and gneissic relicts, with the latter fading into the former (fig. 2), and the occurrence of garnet in the leucosome and concentrated at gneiss margins are compelling textural evidence that the leucosome formed in situ by a vapor-absent (dehydration) biotite breakdown/melting reaction of the type:



in which garnet is a solid product of the reaction (Powell and Downes 1990) along with a melt. Melt reactions of this type are commonly inferred to occur in high-grade terranes in quartz – biotite – plagioclase  $\pm$  sillimanite assemblages (e.g., Thompson 1982; Clemens and Vielzeuf 1987; Patiño Douce and Johnston 1991; Otamendi et al. 1999). Such reactions have been experimentally confirmed by numerous workers (Le Breton and Thompson 1988; Vielzeuf and Holloway 1988; Patiño Douce and Johnston 1991; Vielzeuf and Montel 1994; Carrington and Harley 1995; Gardien et al. 1995).

The primary difference between compositions of protoliths in the experimental studies and the present case is that quartz is not present in the gneisses and is present only sparingly in the leucosome shown in figure 2 (and is not included as a reactant phase in reaction 1). Leucosomes contain ~52 wt%  $\text{SiO}_2$  and gneisses ~46 wt%  $\text{SiO}_2$ . Quartz usually constitutes 20%–30% of the protolith mode in the experimental studies. Experimentally generated melts from systems containing quartz are highly silicic (~65–70 wt%  $\text{SiO}_2$ ) and contain a K-feldspar component that crystallizes as phenocrysts or is dissolved as orthoclase component in plagioclase

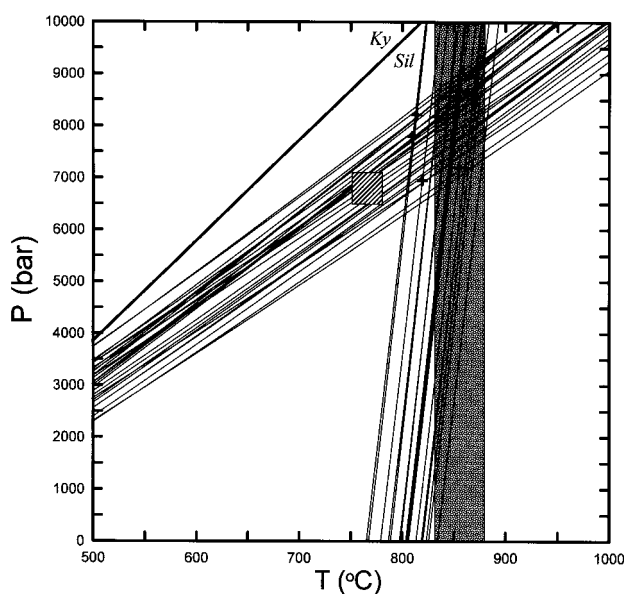


**Figure 11.** Results of all garnet-biotite (GARB)/garnet-aluminosilicate-quartz-plagioclase (GASP) thermobarometry for 12 samples of sillimanite-bearing migmatitic gneisses from the Winding Stair Gap outcrop, including gneiss and leucosome in figure 2. The steep lines correspond to the P-T locus of garnet-biotite Fe-Mg exchange equilibria based on the composition of garnet cores and biotite inclusions in feldspar near the corresponding garnet. Shallower lines are the locus of GASP for garnet core and matrix plagioclase compositions. The average GASP and GARB intersection is  $850^{\circ} \pm 20^{\circ}\text{C}$  and  $8.0 \pm 0.6$  kbar (both  $1\sigma$ ). Plus symbols correspond to the intersection of GASP and GARB for garnet-biotite-plagioclase from the same sample used to calculate the average. Small shaded box is peak P-T calculated by Absher and McSween (1985) using matrix biotite for GARB. Vertical shaded box delimits the T range obtained from garnet-K-feldspar, sillimanite-K-feldspar (Moecher and Sharp 1999), and garnet-plagioclase oxygen isotope temperatures (this study).

solid solutions (Vielzeuf and Holloway 1988; Patiño Douce and Johnston 1991). Vapor absent melting of the biotite- and quartz-bearing experimental systems typically begins at  $\sim 750^{\circ}\text{C}$ , with the greatest proportion of melt generated at  $850^{\circ}\text{--}900^{\circ}\text{C}$  (e.g., Vielzeuf and Holloway 1988; Gardien et al. 1995), which is the temperature range in the present case based on geothermobarometry.

Although biotite dehydration melting is potentially a viable mechanism for explaining the generation of a garnet-bearing melt, the WSG leucosomes are nowhere near a ternary granite minimum system, whereas experimental melts tend to more closely approximate the minimum

composition. However, such a composition would not be expected from melting of a highly aluminous, quartz-absent Bt-Sil-Plag-Grt gneiss (Patiño Douce and Johnston 1991). We propose that the WSG leucosome could result from biotite dehydration melting of high-grade gneisses similar to those included in the leucosome (albeit with higher initial silica contents), followed by fractionation and expulsion of a more felsic component from the leucosome. In fact, many leucocratic veins in migmatites are tonalitic to trondhjemitic, lacking significant K-feldspar as a discrete phase. These leucosomes are inferred to have undergone a phase of physical fractionation in which a granitic component separates from the melt, leaving the plagioclase-rich leucosome (Sawyer 1996, 1998). This process is supported by the presence of aggregates of euhedral plagioclase containing interstitial quartz (fig. 3b). Any  $\text{K}_2\text{O}$  generated by biotite breakdown and not lost in a more felsic melt fraction could be incorporated as an orthoclase component in plagioclase on initial crystallization of the melt (Patiño Douce and Johnston 1991; Vielzeuf and Montel 1994) and then exsolved to form antiperthite, as is visible in the present case (fig. 3b). In comparison, the composition (high Al, Fe, Ca and low Si, K) and mineralogy (abundant sillimanite, garnet, plagioclase; lack of muscovite) of the gneiss support the inference that the gneiss is restitic material whose composition results from the melting event that generated the leucosomes and possibly an earlier muscovite dehydration melting event.

Biotite breakdown explains the presence of rutile in the leucosome, which formed from the  $\text{TiO}_2$  released by biotite. The presence of garnet with sillimanite inclusions is accounted for by formation of new garnet in part from biotite components during initial reaction. New garnet growth, as opposed to simply retaining protolith garnet in the melt, is supported by (1) the contrast in shape and size between gneissic and leucosome garnet and (2) the fact that the coarsest leucosome garnets also exhibit a distinctly different compositional zoning pattern with high Ca cores that contrast with the lower Ca rims of leucosome garnet and to the low Ca garnet in gneiss. The strong linear fabric in gneisses, expressed in part as the elliptical garnet shapes evident in figure 2 (*inset 4*), and the widespread presence of boudinage of gneiss in the slab and elsewhere in the outcrop imply a component of elongation strain preceded and perhaps attended by the early stages of melting, providing avenues for focusing of melt migration.

**Zircon Formation.** We interpret the zircon to be directly related to leucosome formation, rather

than being relict zircons from the gneiss, because (1) the gneissic protoliths contain far fewer and much smaller zircons; (2) the zircons in the leucosome contain none of the complex zoning typical of zircons with Proterozoic inheritance found in other samples at WSG (Miller et al. 1998); (3) the zircons exhibit a faint but simple concentric zoning typical of igneous zircon and an unzoned rim related to metamorphic or subsolidus annealing (Moecher and Miller 2000; fig. 4*d*); and (4) in contrast to zircons from pelitic gneiss at WSG, which invariably had Proterozoic cores, only two grains among 39 analyzed from the leucosome had a pre-Ordovician core. That said, the high Zr concentration (and zircon abundance) requires a physical concentration of new zircon grains at some stage in the evolution of the leucosome. The Zr concentration and zircon growth must have occurred early because zircon occurs as inclusions in garnet and in the center of plagioclase phenocrysts (fig. 3*a–c*).

A complete assessment of the origin of the abundant zircon in the leucosomes is beyond the scope of this study, and we can only speculate as to the reason for this abundance. Because the theoretical solubility of Zr in the leucosome is much lower than the measured Zr concentration, we envision a physical concentration of newly grown zircon crystals in the leucosome. New zircon must have then nucleated and grown in the melt, followed by its inclusion in newly nucleated garnets and then inclusion by nucleating plagioclase. That few of the

original zircons were entrained in the extracted melt is demonstrated by the rarity of pre-Taconian ages determined by TIMS and ion microprobe. The clusters of zircons evident in thin section (fig. 4) suggest that agglomeration of zircon occurred before enclosure by garnet and plagioclase; this pattern potentially corresponds to a period of fractional crystallization of zircon. Melt remaining after crystallization of plagioclase was expelled, leaving the largely quartz diorite to diorite leucosome with a nonequilibrium Zr concentration for the present rock composition. Assuming derivation of a felsic melt (table 1) from a protolith approaching the gneiss in composition and Zr saturation of that melt, a melt-leucosome ratio of approximately 10 : 1 would be required to generate the Zr concentration of the leucosome. Further evaluation and testing of this model requires additional sampling, major and trace element analysis, and assessment of the distribution of zircon in the gneiss.

#### ACKNOWLEDGMENTS

We appreciate the contribution of I. Ridley and E. Haynes (USGS), who provided the LA-ICPMS analyses of garnet. B. Watson and F. Bea provided helpful journal reviews. We acknowledge National Science Foundation (NSF) grant EAR-0106853 to S. Samson, NSF EAR-9814801 to C. F. Miller, and NSF IF-0001322 to D. P. Moecher in support of the UK electron probe microanalyzer.

#### REFERENCES CITED

- Absher, S. A., and McSween, H. Y. 1985. Granulites at Winding Stair Gap, North Carolina: the thermal axis of Paleozoic metamorphism in the southern Appalachians. *Geol. Soc. Am. Bull.* 96:588–599.
- Berman, R. G. 1991. Thermobarometry using multi-equilibrium calculations: a new technique, with petrological applications. *Can. Mineral.* 29:833–855.
- Bindeman, I. N.; Vinogradov, V. I.; Valley, J. W.; Wooden, J. L.; and Natal'in, B. A. 2002. Archean protolith and accretion of crust in Kamchatka: SHRIMP dating of zircons from Sredinny and Ganal Massifs. *J. Geol.* 110: 271–289.
- Bottinga, Y., and Javoy, M. 1973. Comments on oxygen isotope geothermometry. *Earth Planet. Sci. Lett.* 20: 250–265.
- Butler, R. D. 1972. Age of Paleozoic regional metamorphism in the Carolinas, Georgia, and Tennessee southern Appalachians. *Am. J. Sci.* 272:319–333.
- Carpenter, R. H. 1970. Metamorphic history of the Blue Ridge province of Tennessee and North Carolina. *Geol. Soc. Am. Bull.* 81:749–761.
- Carrigan, C. W.; Miller, C. F.; Fullager, P. D.; Bream, B. R.; Hatcher, R. D.; and Coath, C. D. 2003. Ion microprobe age and geochemistry of southern Appalachian basement, with implications for Proterozoic and Paleozoic reconstructions. *Precambrian Res.* 120:1–36.
- Carrington, D. P., and Harley, S. L. 1995. Partial melting and phase relations in high-grade metapelites: an experimental petrogenetic grid in the KFMASH system. *Contrib. Mineral. Petrol.* 120:270–291.
- Cherniak, D. J., and Watson, E. B. 2001. What are we dating? understanding the crystallogenes of U-Pb geochronometers. *Chem. Geol.* 172:5–24.
- Clemens, J. D., and Vielzeuf, D. 1987. Constraints on melting and magma production in the crust. *Earth Planet. Sci. Lett.* 86:287–306.
- Connelly, J. B., and Dallmeyer, R. D. 1993. Polymetamorphic evolution of the western Blue Ridge: evidence from  $^{40}\text{Ar}/^{39}\text{Ar}$  whole-rock slate/phyllite and muscovite ages. *Am. J. Sci.* 293:322–359.
- Couture, R. A.; Smith, M. S.; and Dymek, R. F. 1993. X-ray fluorescence analysis of silicate rocks using fused glass discs and a side-window Rh source tube: accu-

- racy, precision and reproducibility. *Chem. Geol.* 110: 315–328.
- Dallmeyer, R. D. 1975. Incremental  $^{40}\text{Ar}/^{39}\text{Ar}$  ages of biotite and hornblende from retrograded basement gneisses of the southern Blue Ridge: their bearing on the age of Paleozoic metamorphism. *Am. J. Sci.* 275: 124–149.
- Donahue, C. L.; Manning, C. E.; and Essene, E. J. 2001. The pressure and temperature dependence of Zr and Ti substitution in almandine. *Geol. Soc. Am. Abstr. Program* 33:251.
- Drake, A. A.; Sinha, A. K.; Laird, J.; and Guy, R. E. 1989. The Taconic orogen. *In* Hatcher, R. D., Jr.; Thomas, W. A.; and Viele, G. W., eds. *The Appalachian-Ouachita orogen in the United States*. *Geol. Soc. Am. DNAG, Ser. F-2*, p. 101–177.
- Eckert, J. O., Jr.; Hatcher, R. D., Jr.; and Mohr, D. W. 1989. The Wayah granulite-facies metamorphic core, southwestern North Carolina: high grade culmination of Taconic metamorphism in the southern Blue Ridge. *Geol. Soc. Am. Bull.* 101:749–762.
- Eiler, J. M.; Valley, J. W.; and Baumgartner, L. P. 1993. A new look at stable isotope thermometry. *Geochim. Cosmochim. Acta* 57:2571–2583.
- Farquhar, J.; Chacko, T.; and Frost, B. R. 1993. Strategies for high-temperature oxygen isotope thermometry: a worked example from the Laramie anorthosite complex, Wyoming, USA. *Earth Planet. Sci. Lett.* 117:407–422.
- Fraser, G.; Ellis, D.; and Eggins, S. 1997. Zirconium abundance in granulite facies minerals, with implications for zircon geochronology in high grade rocks. *Geology* 25:607–610.
- Gardien, V.; Thompson, A. B.; Grujic, D.; and Ulmer, P. 1995. Experimental melting of biotite + plagioclase + quartz + muscovite assemblages and implications for crustal melting. *J. Geophys. Res.* 100:15,581–15,591.
- Giletti, B. 1986. Diffusion effects on oxygen isotope temperatures of slowly cooled igneous and metamorphic rocks. *Earth Planet. Sci. Lett.* 77:218–228.
- Glover, L., III; Speer, A.; Russell, G. S.; and Farrar, S. S. 1983. Ages of regional metamorphism and ductile deformation in the central and southern Appalachians. *Lithos* 16:223–245.
- Hatcher, R. D., Jr. 1987. Tectonics of the southern and central Appalachian internides. *Annu. Rev. Earth Planet. Sci.* 15:337–362.
- Hatcher, R. D., Jr., and Butler, J. R. 1979. Guidebook for southern Appalachian field trip in the Carolinas, Tennessee, and northeastern Georgia. *In* International Geological Correlation Program, Caledonide Orogen Prog. 27 Field Trip, 117 p.
- Horton, J. W., Jr.; Drake, A. A., Jr.; and Rankin, D. W. 1989. Tectonostratigraphic terranes and their Paleozoic boundaries in the central and southern Appalachians. *In* Dallmeyer, D., ed. *Terranes in the circum-Atlantic Paleozoic orogens*. *Geol. Soc. Am. Spec. Pap.* 230:213–245.
- Hoskin, P. W. O., and Black, L. P. 2000. Metamorphic zircon formation by solid-state recrystallization of protolith igneous zircon. *J. Metamorph. Geol.* 18:423–439.
- Kish, S. A. 1991. Potassium-argon dating in the western Blue Ridge of North Carolina and Tennessee. *In* Kish, S. A., ed. *Studies of Precambrian and Paleozoic stratigraphy in the western Blue Ridge*. *Carolina Geol. Soc. Guidebook*, p. 69–77.
- Le Breton, N., and Thompson, A. B. 1988. Fluid-absent (dehydration) melting of biotite in metapelites in the early stages of crustal anatexis. *Contrib. Mineral. Petrol.* 99:226–237.
- Ludwig, K. R. 1988. PBDAT for MS-DOS: a computer program for IBM-PC compatibles for processing raw Pb-U-Th isotope data. *U.S. Geol. Surv. Open File Rep.* OF 88–0542.
- Miller, B. V.; Stewart, K. G.; Miller, C. F.; and Thomas, C. W. 2000a. U-Pb ages from the Bakersville, North Carolina eclogite: Taconian eclogite metamorphism followed by Acadian and Alleghanian cooling. *Geol. Soc. Am. Abstr. Program* 32:62.
- Miller, C. F.; Hatcher, R. D., Jr.; Ayers, J. C.; Coath, C. D.; and Harrison, T. M. 2000b. Age and zircon inheritance of eastern Blue Ridge plutons, southwestern North Carolina and northeastern Georgia with implications for magma history and evolution of the southern Appalachian orogen. *Am. J. Sci.* 300:142–172.
- Miller, C. F.; Hatcher, R. D., Jr.; Harrison, T. M.; Coath, C. D.; and Gorisch, E. B. 1998. Cryptic crustal events elucidated through zone imaging and ion microprobe studies of zircon, southern Appalachian Blue Ridge, North Carolina-Georgia. *Geology* 26:419–422.
- Moecher, D. P. 1999. Kyanite-sillimanite-melt relationships at Winding Stair Gap, NC: constraints on the Taconian granulite facies P-T path of the southern Blue Ridge. *Geol. Soc. Am. Abstr. Program* 31:31.
- Moecher, D. P., and Miller, C. F. 2000. Precise age for peak granulite facies metamorphism and melting in the eastern Blue Ridge from SHRIMP U-Pb analysis of zircon. *Geol. Soc. Am. Abstr. Program* 32:63.
- Moecher, D. P., and Sharp, Z. D. 1999. Comparison of conventional and garnet-aluminosilicate-quartz O isotope thermometry: insights for mineral equilibration in metamorphic rocks. *Am. Mineral.* 84:1287–1303.
- Moecher, D. P.; Tracy, R. J.; and Anderson, E. D. 2003. Taconian metamorphism in eastern Great Smoky Mountains inferred from U-Th-Pb monazite chemical ages. *Geol. Soc. Am. Abstr. Program* 35:20.
- Otamendi, J. E.; Patiño Douce, A. E.; and Demichelis, A. H. 1999. Amphibolite to granulite transition in aluminous greywackes from the Sierra de Comechingones, Cordoba, Argentina. *J. Metamorph. Geol.* 17: 415–434.
- Ownby, S. E.; Miller, C. F.; Berquist, P. J.; Carrigan, C. W.; and Fullagar, P. D. 2004. Geochemistry and U-Pb geochronology of a portion of the Mars Hill Terrane, North Carolina-Tennessee: constraints on origin, history, and tectonic assembly. *In* Tollo, R. P.; Corriveau, L.; McLelland, J.; and Bartholomew, M. J., eds. Pro-

- terozoic evolution of the Grenville orogen in North America. *Geol. Soc. Am. Mem.* 197:609–632.
- Patiño Douce, A. E., and Beard, J. S. 1995. Dehydration melting of biotite gneiss and quartz amphibolite from 3 to 15 kbar. *J. Petrol.* 36:707–738.
- Patiño Douce, A. E., and Johnston, A. D. 1991. Phase equilibria and melt productivity in the pelitic system: implications for the origin of peraluminous granitoids and aluminous granulites. *Contrib. Mineral. Petrol.* 107:202–218.
- Patiño Douce, A. E.; Johnston, A. D.; and Rice, J. M. 1993. Octahedral excess mixing properties in biotite: a working model with applications to geobarometry and geothermometry. *Am. Mineral.* 78:113–131.
- Powell, R., and Downes, J. 1990. Garnet porphyroblast bearing leucosomes in metapelites. *In* Ashworth, J. R., and Brown, M., eds. *High temperature metamorphism and anatexis*. Unwin-Hyman, London, p. 105–123.
- Roberts, M. P., and Finger, F. 1997. Do U-Pb zircon ages from granulites reflect peak metamorphic conditions? *Geology* 25:319–322.
- Samson, S. D., and D’Lemos, R. S. 1998. U-Pb geochronology and Sm-Nd isotopic composition of Proterozoic gneisses, Channel Islands, UK. *J. Geol. Soc. Lond.* 155:609–618.
- Sawyer, E. W. 1996. Melt segregation and magma flow in migmatites: implications for the generation of granite magmas. *Trans. R. Soc. Edinb. Earth Sci.* 87:85–94.
- . 1998. Formation and evolution of granite magmas during crustal reworking: the significance of diatexites. *J. Petrol.* 39:1147–1167.
- Schaltegger, U.; Fanning, C. M.; Gunther, D.; Maurin, J. C.; Schulmann, K.; and Gebauer, D. 1999. Growth, annealing and recrystallization of zircon and preservation of monazite in high-grade metamorphism: conventional and in-situ isotope, cathodoluminescence and microchemical evidence. *Contrib. Mineral. Petrol.* 134:186–201.
- Sharp, Z. D. 1995. Oxygen isotope geochemistry of the  $\text{Al}_2\text{SiO}_5$  polymorphs. *Am. J. Sci.* 295:1058–1076.
- Sinha, A. K. 1997. The duration of the Taconic orogeny in the central Appalachians. *Geol. Soc. Am. Abstr. Program* 29:69.
- Spear, F. S., and Florence, F. P. 1992. Thermobarometry in granulites: pitfalls and new approaches. *Precambrian Res.* 55:209–241.
- Spear, F. S.; Kohn, M. J.; and Cheney, J. T. 1999. P-T paths from anatectic pelites. *Contrib. Mineral. Petrol.* 134:17–32.
- Stacey, J. S., and Kramers, J. D. 1975. Approximation of terrestrial lead isotope evolution by a two-stage model. *Earth Planet. Sci. Lett.* 26:207–221.
- Thompson, A. B. 1982. Dehydration melting of pelitic rocks and the generation of  $\text{H}_2\text{O}$ -undersaturated granitic liquids. *Am. J. Sci.* 282:1567–1595.
- Thompson, A. B., and England, P. C. 1984. Pressure-temperature-time paths of regional metamorphism. II. Their influence and interpretation using mineral assemblages in metamorphic rocks. *J. Petrol.* 25:929–955.
- Tucker, R. D.; Krogh, T. E.; Ross, R. J., Jr.; and Williams, S. H. 1990. Time-scale calibration by high-precision U-Pb zircon dating of interstratified volcanic ashes in the Ordovician and Lower Silurian stratotypes of Britain. *Earth Planet. Sci. Lett.* 100:51–58.
- Vielzeuf, D., and Holloway, J. R. 1988. Experimental determination of the fluid-absent melting relations in the pelitic system. *Contrib. Mineral. Petrol.* 98:257–276.
- Vielzeuf, D., and Montel, J. M. 1994. Partial melting of metagreywackes. I. Fluid absent experiments and phase relationships. *Contrib. Mineral. Petrol.* 117:375–393.
- Watson, E. B. 1996. Dissolution, growth and survival of zircons during crustal fusion: kinetic principles, geological models and implications for isotopic inheritance. *Trans. R. Soc. Edinb. Earth Sci.* 87:43–56.
- Watson, E. B., and Harrison, T. M. 1983. Zircon saturation revisited: temperature and composition effects in a variety of crustal magma types. *Earth Planet. Sci. Lett.* 64:295–304.
- Winther, K. T. 1996. A model for estimating the composition of partial melts. *Mineral. Petrol.* 53:189–195.